# Co-Located Wind and Temperature Observations at Mid-Latitudes During Mesospheric Inversion Layer Events

Alexis Mariaccia, Philippe Keckhut, Alain Hauchecorne, Sergey Khaykin, Mathieu Ratynski

Geophysical Research Letters

RESEARCH LETTER
10.1029/2022GL102683

# Co-Located Wind and Temperature Observations at Mid-Latitudes During Mesospheric Inversion Layer Events

**A. Mariaccia[1], P. Keckhut[1], A. Hauchecorne[1], S. Khaykin[1], and M. Ratynski[1]**

[1]Laboratoire Atmosphères, Milieux, Observations Spatiales, UMR 8190, Institut Pierre-Simon Laplace, Université Versailles-Saint Quentin, Université Paris-Saclay, Guyancourt, France

**Key Points:**

- First simultaneous wind and temperature observations in the altitude range 30–90 km during mesospheric inversion layer events
- According to these new observations, there is a strong wind deceleration occurring at the same altitude that the temperature inversion
- These results argue in favor of the mesospheric inversion layer's formation mechanism involving gravity wave dissipation

**Correspondence to:**

A. Mariaccia,
alexis.mariaccia@latmos.ipsl.fr

**Citation:**

Mariaccia, A., Keckhut, P., Hauchecorne, A., Khaykin, S., & Ratynski, M. (2023). Co-located wind and temperature observations at mid-latitudes during mesospheric inversion layer events. *Geophysical Research Letters*, *50*, e2022GL102683. https://doi.org/10.1029/2022GL102683

Received 5 JAN 2023
Accepted 24 FEB 2023

**Author Contributions:**

**Conceptualization:** A. Mariaccia, P. Keckhut, A. Hauchecorne, S. Khaykin
**Investigation:** A. Mariaccia
**Methodology:** A. Mariaccia, P. Keckhut, A. Hauchecorne, S. Khaykin
**Software:** A. Mariaccia
**Supervision:** P. Keckhut, A. Hauchecorne, S. Khaykin
**Validation:** P. Keckhut, A. Hauchecorne, S. Khaykin, M. Ratynski
**Visualization:** A. Mariaccia, P. Keckhut, A. Hauchecorne, M. Ratynski
**Writing – original draft:** A. Mariaccia
**Writing – review & editing:** P. Keckhut, A. Hauchecorne, S. Khaykin, M. Ratynski



**Abstract** The mesospheric inversion layer (MIL) phenomenon is a temperature enhancement (10–50 K) in a vertical layer (~10 km) lasting several days and spanning thousands of kilometers within the mesosphere. As MILs govern the mesospheric variability, their study is crucial for a better understanding of the middle-atmosphere global circulation. MIL phenomenon is also important for applications in aeronautics as perturbations in the mesosphere are significant issues for the safe reentry of rockets, space shuttles, or missiles. However, the description of this phenomenon remains incomplete, since no observations of MIL's effects on winds exist, hampering an understanding of the mechanisms responsible for their formation. This study investigates simultaneous wind-temperature observations in the altitude range of 30–90 km during MIL events. Strong winds deceleration occurred in the same altitude range as the temperature inversion, confirming the role of gravity waves in MIL's formation mechanisms.

**Plain Language Summary** Atmospheric waves propagate from the lower to upper layers, transferring their energy throughout the atmosphere. The mesosphere (50–90 km) is subject to these energy transfers, causing unexpected temperature increases (10–50 K) over a vertical layer (~10 km). These deviations are called mesospheric inversion layers (MILs). Though largely observed in temperature profiles, the MIL phenomenon remains misunderstood, as MIL's impacts on the wind in the middle atmosphere remain unknown. In this study, we first reported simultaneous wind-temperature observations between 30 and 90 km during MIL events. We observed a strong wind deceleration in the same altitude range where the temperature increases. This result argues in favor of the role of gravity waves in MIL's formation mechanisms.

## 1. Introduction

The mesosphere (50–90 km) is a substantial layer of the atmosphere where large and small-scale perturbations occur. These perturbations are caused by the propagation and breaking of atmospheric tides and waves from sources above and below, inducing deviations from its natural thermal structure. The so-called Mesospheric Inversion Layer (MIL) phenomenon is an especially significant perturbation that is now recognized to be responsible for a large part of the mesospheric variability. Moreover, MILs have garnered interest among researchers, since mesospheric perturbations are significant issues for applications in aeronautics, in particular the safe reentry of space shuttles and missiles (Wing et al., 2020). Indeed, since the first MIL phenomenon's signatures observed by rockets (e.g., Schmidlin, 1976; Stroud et al., 1960; Theon et al., 1967) that reported a non-expected positive lapse rate in the mesosphere, researchers have carried out numerous studies of MIL events (e.g., Cutler et al., 2001; Dao et al., 1995; Duck et al., 2001; Gan et al., 2012; Leblanc et al., 1995; Leblanc & Hauchecorne, 1997). An important review of the knowledge state on the MIL phenomenon has been carried out by Meriwether and Gardner (2000). The MIL phenomenon (henceforth referred to as simply MIL) is defined as a layer of about 10 km with enhanced temperature between 15 and 50 K, spanning over a thousand square kilometers over several days. MILs are currently known to occur quite often at low to mid-latitudes, preferentially in winter, and have been separated into two subtypes: the lower MIL, occurring between 65 and 80 km, especially in winter, and the upper MIL, occurring above 85 km. Different mechanisms have been suggested to explain their formation, such as planetary waves dissipation (France et al., 2015; Salby et al., 2002), gravity waves and tides interaction (Liu & Hagan, 1998; Meriwether & Gardner, 2000), and chemical heating (Meriwether & Mlynczak, 1995; Ramesh et al., 2013); however, these mechanisms remain not entirely described and are still an active research field. In particular, the wind behavior in the middle atmosphere (30–90 km) when a MIL event occurs remains an unanswered question, even though several studies have suggested its significant role in the MIL appearance (Meriwether & Gerrard, 2004). For instance, Hauchecorne et al. (1987) estimated the

role of gravity wave dissipation in the MIL's persistence, and showed that this process strongly depends on the temperature and the background wind. Salby et al. (2002) and Sassi et al. (2002) cfocused on the mechanism of MIL creation and revealed with simulations that the planetary wave breaking is supposed to occur in the same altitude range of a weak zonal wind region. The wind behavior during MIL events is an essential component of understanding the MIL phenomenon and, more broadly, the impacts on general middle atmosphere circulation. Although some studies have reported simultaneous wind-temperature observations in the middle atmosphere (e.g., Baumgarten, 2010; Stroud et al., 1960; Theon et al., 1967), most of them did not focus on the MIL phenomenon. Furthermore, some of these studies have detected MILs without knowing the phenomenon. For instance, Stroud et al. (1960) was unaware of the MIL phenomenon yet reported a temperature inversion at 80 km with strong wind shear at the same altitude without giving any explanation to this observed behavior.

Despite this supposed role, only two studies Huang et al. (1998), Huang et al. (2002) have reported simultaneous zonal wind and temperature observations from Na LiDAR in the altitude range 85–100 km in which a large wind shear associated with a MIL was detected. However, this incomplete description of the wind signature at upper MIL altitudes is insufficient for determining the entire shear profile and studying how gravity waves propagate from the stratosphere to the thermosphere (Le Du et al., 2022).

To date, all the theoretical and modeled wind behavior assumptions in the middle atmosphere during a MIL event have never been confirmed due to the absence of accurate co-located and simultaneous temperature and wind measurements with the former instruments (Meriwether & Gerrard, 2004). To our knowledge, the DYANA campaign, which took place in the northern hemisphere in 1990, is one the only during which Rayleigh LiDAR and falling spheres simultaneously measured temperature and wind, respectively, in the whole middle atmosphere. However, the characteristics of the MILs observed during this campaign were not studied, as this was not one of the main objectives. In addition, the falling sphere profiles suffer from significant smoothing and bias (see Figure 1) due to the large speed of the payload in the mesosphere, making this technique not enough reliable (Lübken et al., 1994). Since then, remote sensing techniques have been developed, particularly with the rise of the Doppler Rayleigh LiDAR technology capable of accurately measuring the temperature and wind in the atmospheric window of 30–90 km. Doppler LiDAR currently operates at the Observatoire of Haute-Provence (OHP) as well as Rayleigh LiDAR and Ozone LiDAR. The latter two LiDAR measuring the temperature and monitoring the ozone, respectively, making the OHP one of the rare station in the world where co-located and simultaneous wind-temperature observations in the middle-atmosphere are possible.

Our study aims to answer how the winds evolve during MIL events by providing the first time simultaneous temperature and wind observations in the altitude range of 30–90 km. The two observation data sets used here were acquired at Biscarrosse during the DYANA campaign in 1990 and at the OHP, located 550 km apart, in 2021/2022 winter. Biscarrosse and OHP stations exhibit a similar mesospheric climatology (Hauchecorne et al., 1991), making them well-situated for investigating the MIL's signature at both sites. Additionally, we explore how ERA5 reanalyzes simulated the wind and temperature during MIL events.

The publication is structured as follows. In Section 2, the data set from DYANA and Aeolus Validation campaigns as well as ERA5 reanalyzes are presented. Then, the method to identify and to characterize MIL events is described in Section 3. The temperature-wind observations for each selected date with MIL events are shown and commented in Section 4. Finally, mechanisms responsible for lower MILs are discussed, and perspectives are given in Section 5.

## 2. Data Description

### 2.1. The DYANA Campaign: Rayleigh LiDAR and Falling Spheres

The DYANA (DYnamics Adapted Network for the Atmosphere) campaign was conducted in the northern hemisphere over a large horizontal area from January to March 1990 in order to explore the middle atmosphere dynamics (10–100 km). This campaign was designed to improve the lack of horizontal coverage missing during previous campaigns. The main dynamical objectives were to study the large, medium, and small-scale variations generated by planetary waves, gravity waves, tides, and turbulence. Another aim was to inter-compare measurements in order to cross-check experimental methods. Thus, several techniques were employed during these 3 months to measure temperature and density from multiple ground-based stations. The set of these techniques with their monitored height range was: rocket bornes (90–115 km), falling spheres (30–90 km), Rayleigh LiDAR

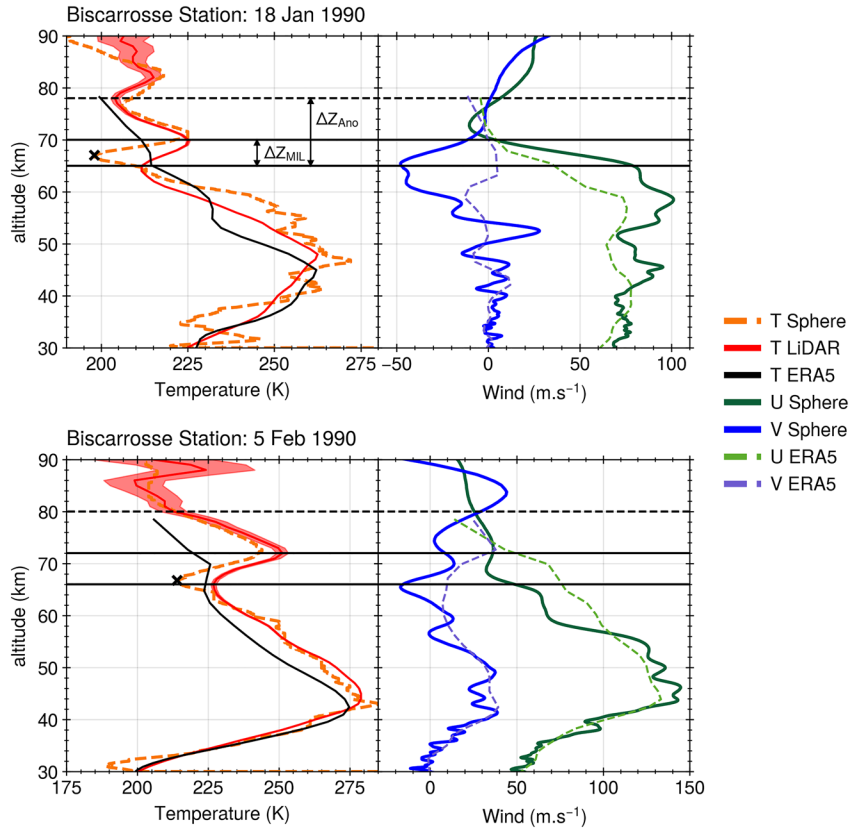


**Figure 1.** Temperature and wind profiles measured at Biscarrosse from falling spheres and Rayleigh LiDAR between 30 and 90 km for two dates during the DYANA Campaign. The statistical noise (red shaded area) of the LiDAR temperature signal is displayed. The two horizontal black solid lines indicate, respectively, the derived bottom and top of the MIL detected by the Rayleigh LiDAR. The horizontal dashed line represents the altitude of the potential total extension of the temperature anomaly ($\Delta Z_{Ano}$). The black cross points out the bottom of the MIL measured from falling spheres. In addition, the ERA5 temperature-wind profiles extracted for each date are shown.

(30–90 km), sodium LiDAR (80–105 km), data sondes (25–65 km) and radiosondes (0–32 km). These different instruments occasionally carried out coordinated temperature and density measurements at the exact location and approximately the same periods (about 1 hr) to perform inter-comparisons. For instance, the station based in southwest France at Biscarrosse (44°N–1°W) benefited from simultaneous observations from Rayleigh LiDAR and falling spheres. During the campaign, falling spheres were released at about 110 km altitude to obtain density, temperature, and wind profiles in the middle atmosphere. A detailed description of the falling sphere technique can be found in Engler (1965) and Jones and Peterson (1968). At the ground, a Rayleigh LiDAR measured the density profile by counting the number of photons from which the temperature was inferred by assuming hydrostatic equilibrium in the 30–90 km range, where a pure molecular backscattering is expected. The vertical resolution of LiDAR temperature profiles is typically 200 m. The Rayleigh Lidar method and the technical information about the LiDAR located at Biscarrosse have been described in Hauchecorne et al. (1991). The complete description of the DYANA campaign and its objectives have been reported in Offermann (1994). The presentation of each instrumental technique and the inter-comparison results are shown in Lübken et al. (1994). In the measurements data set carried out at Biscarrosse in 1990, eight dates of co-located and simultaneous temperature-wind observations are available.

### 2.2. Aeolus Validation Campaign: OHP LiDARs

In August 2018, in the frame of the Living Planet Program, the Aeolus satellite was launched by the European Space Agency in order to provide global wind profiles from the surface to 30 km for a 3 years period (Straume et al., 2020). The Aeolus satellite measures horizontal line-of-sight winds with a Doppler wind LiDAR named

ALADIN (Atmospheric LAser Doppler Instrument), which is the first-ever Doppler Wind LiDAR embarked on a satellite. In the meantime and in order to assess and validate Aeolus wind observations, ground-based Doppler LiDAR observations within the AboVE-2 (Aeolus Validation Experiment) were undertaken at the Observatory of Haute-Provence (OHP, 44°N, 6°E) (Ratynski et al., 2022). Moreover, the double-edge technique for wind profiling, first demonstrated at OHP (Chanin et al., 1989; Garnier et al., 1992), is realized in ALADIN Rayleigh channel. Several co-located LiDARs have been monitoring the middle atmosphere at the OHP within the Network for the Detection of Composition Changes (NDACC) for decades. Since 1993, a LIOvent Doppler LiDAR has been measuring the wind velocities at OHP, providing the first lidar-based wind climatology in the middle atmosphere (Souprayen et al., 1999). The principle, using the Rayleigh backscattering at 532 nm, is based on the Doppler shift between the emitted and the backscattered laser light caused by the displacement of scattering molecules relative to the LiDAR. The detection of Doppler shift is performed employing a double-edge Fapbry-Perot interferometer. The complete description of the Doppler LiDAR's technique and the instrument design at OHP has been reported in Chanin et al. (1989) and more recently in Khaykin et al. (2020).

Finally, an Ozone LiDAR has been monitoring the ozone as part of the Network for the Detection of Stratospheric Changes. The Ozone LiDAR's principle rests on the differential absorption LiDAR technique requiring the emission of two simultaneous laser wavelengths, 308 (absorbing) and 355 (non-absorbing) nm here, with differential absorption by ozone to provide its vertical profile. The method and the technical information about the Ozone LiDAR at OHP have been described in several studies (e.g., Godin-Beekmann et al., 2003; Wing et al., 2018). Thus, in order to perform simultaneous wind and temperature measurements at OHP, the temperature observations can also be derived by the Ozone LiDAR in off mode by using only the non-absorbing channel (355 nm). Therefore, in addition to the DYANA campaign data set, we benefited from 44 dates of simultaneous observations of temperature and wind carried out at the OHP from 2018 to 2022.

### 2.3. ERA5 Reanalyzes

The ERA5 reanalyzes are the last generation of reanalyzes, archiving the past climate on earth from 1950 to the present, produced by the ECMWF (European Center Medium for Weather Forecast) since 2016. These ERA5 reanalyzes are produced with a 4DVar assimilation scheme and the integrated system forecast Cycle 41r2. The ERA5 output is constructed every hour on a 0.25° latitude-longitude grid and 137 vertical levels lying from the surface to the level pressure 0.01 hPa (approximately 80 km). More technical information about ERA5 reanalyzes can be found in Hersbach et al. (2020). Here, in order to pursue investigations on how the ECMWF model simulates the MIL phenomenon already undertaken in Mariaccia et al. (2022), ERA5 wind and temperature reanalyzes are extracted at the nearest hour of the mid of acquisitions for the six dates shown above Biscarrosse and the OHP (Figures 1 and 2).

## 3. Method for Identifying and Characterizing MILs

Here, in order to identify MIL events within the temperature profiles, we followed the method developed by Leblanc and Hauchecorne (1997) and Fechine et al. (2008), which has been applied in numerous previous studies (e.g., Ardalan et al., 2022; Cutler et al., 2001; Leblanc et al., 1998). According to them, a MIL is identified when these three criteria are observed:

- The MIL bottom must be at least 5 km above the stratopause and the MIL top below 90 km.
- The temperature perturbation must be significant relative to the measurement uncertainty, that is, Terr < $\Delta$T.
- Finally, the temperature amplitude must be 2$\sigma$ larger than the temperature fluctuations expected by gravity waves at these altitudes. According to Mzé et al. (2014), gravity waves are expected to generate perturbations of 1.6 K at 50 km and 4 K at 75 km.

Afterward, we characterized each observed MIL by computing their amplitude, thickness, and gradient similarly to the method developed in Figure 2 in Ardalan et al. (2022). Thus, for each observed temperature profile, our algorithm identified two altitudes: the altitude of the bottom MIL from which the temperature gradient reverses and the altitude of the top MIL where the temperature maximum is reached. These two altitudes are pointed out with horizontal solid lines in Figures 1 and 2 which delimit the observed MIL's altitude range ($\Delta Z_{MIL}$). Finally, the altitude corresponding to the potential extension of the temperature anomaly is determined when the temperature profile returns to the standard climatology, which is arbitrarily determined. Thus, amplitudes of temperature

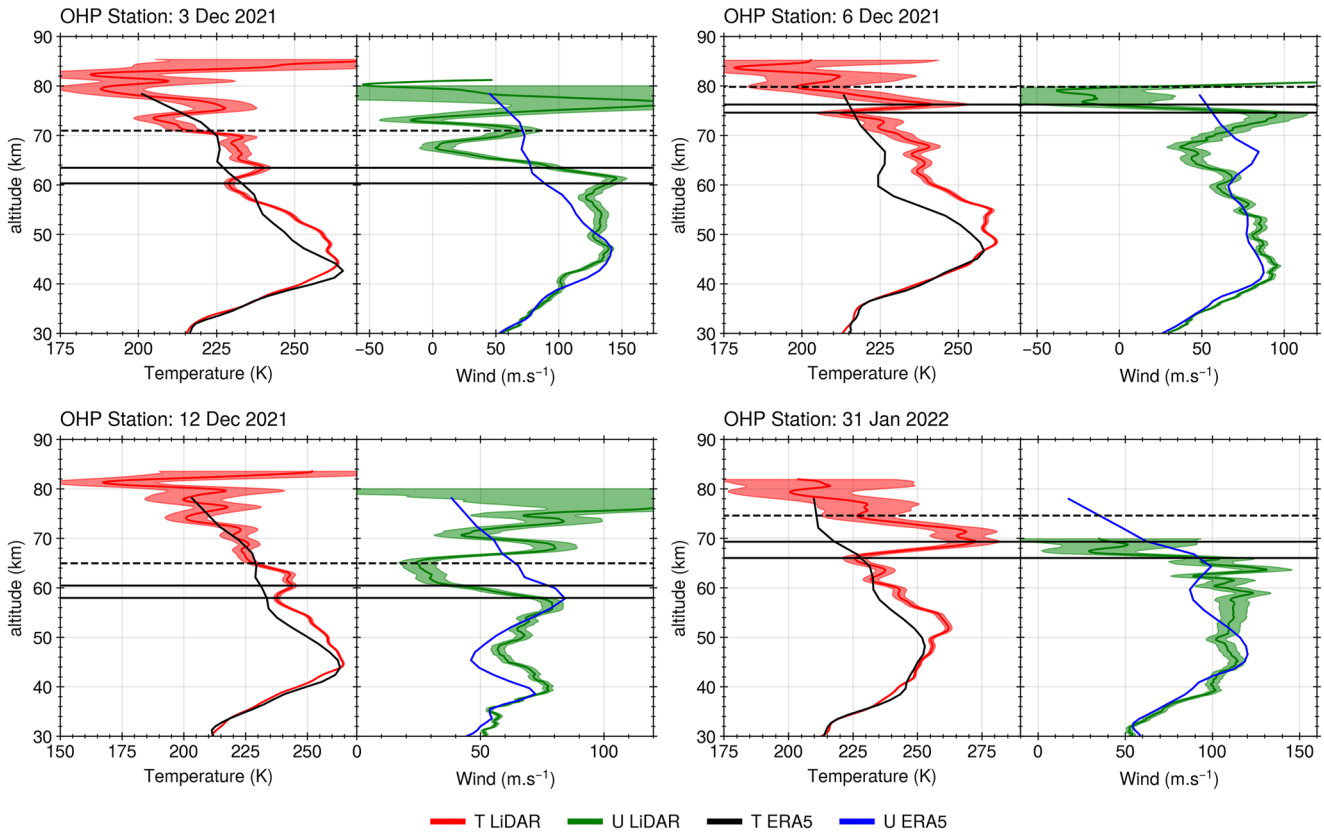


**Figure 2.** Temperature (red) and zonal wind (green) profiles measured for four dates in 2021/2022 winter from the Ozone LiDAR (temperature mode) and the Doppler LiDAR, respectively, located at the OHP. The statistical noise (shaded area) associated with these profiles is displayed. The three horizontal black lines indicate the same MIL's features that in Figure 1. Additionally, ERA5 temperature (black) and wind (blue) reanalyzes profiles are shown for these four dates.

increase ($\Delta T$) within the MIL is computed over the $\Delta Z_{MIL}$ thickness (Figure 1) for each profile. Zonal ($\Delta U$) and meridional ($\Delta V$) wind deviations are computed over the thickness $\Delta Z_{MIL}$ since the reversal of temperature gradients remains a better indicator than a wind drop to identify MIL's signature.

## 4. Results

### 4.1. DYANA Campaign in Biscarrosse

As a result, only two dates in the data from the DYANA campaign possess lower MIL presences which are exploitable. Figure 1 shows temperature zonal and meridional wind profiles measured by LiDAR and falling spheres. Simulated temperature profiles are provided by ERA5 for these two cases in the middle atmosphere during which lower MILs were present. According to these profiles, it is evident that a connection exists between the temperature and wind evolutions, that is, a wind deceleration occurs when the temperature increases, sometimes leading to a wind reversal for both meridional and zonal winds. Moreover, this wind deceleration tends to start at an altitude around the altitude where the temperature inversion starts. For instance, on 18 January 1990, the observed MIL illustrates well this temperature-wind connection with a temperature increase of 13.6 $\pm$ 0.8 K, causing the deceleration of the total wind lying from 92 m.s$^{-1}$ to 12 m.s$^{-1}$. While for the MIL observed on 5 February 1990, a total wind deceleration of around 14 m.s$^{-1}$ is found for a temperature elevation of 24.4 $\pm$ 3 K. Thus, the magnitude of the wind deceleration is not necessarily linearly linked with the temperature amplitude of the MIL. However, these wind deceleration values possess uncertainties since they are computed on the vertical domain where the positive temperature gradient is observed and not in the altitude range where the wind drop occurs. Nevertheless, this method captures the wind deceleration process during a MIL phenomenon.

The temperature measured by the falling sphere is compared with the collocated LiDAR temperature profile for the same dates. As a result, falling spheres' temperatures are systematically lower than LiDAR's temperatures

between 65 and 70–75 km for the two dates. Lübken et al. (1994) have reported that this difference is about 5 K between 65 and 77 km and is mainly due to drag uncertainty associated with the sphere descent that has a significant impact during the transition from super to sub-sonic at these altitudes. Thus, on 18 January 1990, the LiDAR detected the MIL bottom at around 65 km, while the falling sphere temperature profiles exhibit the MIL bottom higher near 68 km. However, the bottom of the MIL observed by the LiDAR corresponds better to the altitude where zonal and meridional winds start to decrease. Furthermore, the temperature profile from the falling spheres possesses a noise not realistic between 30 and 40 km, caused by an effect of vertical winds (Lübken et al., 1994), absent in the LiDAR profile. Therefore, to characterize mesospheric inversions with minimum uncertainty, only the temperature profiles acquired from Rayleigh LiDAR during the DYANA campaign are used to compute MIL's temperature amplitudes.

However, we notice that the ERA5 reanalyzes imprecisely simulated the magnitude, thickness, and altitude of the temperature inversion for these two dates. Surprisingly, for both dates, the zonal and meridional winds deceleration processes associated with the MIL are simulated with realistic magnitudes in ERA5 but starting at lower altitudes than in spheres' observations.

### 4.2. AboVE-2 Campaign at OHP

After applying the MIL identification method to the 44 available temperature profiles, we found only four cases during 2021/2022 winter in which a lower MIL was identifiable.

The main reason for these few identified MIL events is the challenge of measuring wind in the mesosphere due to the dependence on sky transparency. Furthermore, many actual wind observations possess weak signals, limiting the accurate detection of lower MILs during this period. For the recent observations, only zonal wind measurements were performed by the Doppler LiDAR during 2021/2022 winter to facilitate the inter-comparisons with the collocated Aeolus observations, which measures essentially the zonal component of winds. Nevertheless, as the zonal wind is often more significant than the meridional wind in the mesosphere by a factor of 10, we supposed that a zonal wind reduction implies very likely a total wind deceleration.

Figure 2 shows temperature and zonal wind profiles observed above the OHP for these four dates in the mesosphere where lower MILs were detected. Similar zonal wind deceleration behavior, as observed in Figure 1, is found within the lower MILs. In addition, the altitudes at which the temperature increases match well with those where the zonal wind starts to decelerate, similar to previous observations (Figure 1), confirming the temperature-wind connection. Afterward, we computed the MIL's characteristics by following the method described in Section 3 for these four MIL events. For instance, on 3 December 2021, the MIL detected was characterized by a temperature elevation of 11.1 ± 3.9 K associated with a zonal wind deceleration of 43.3 ± 17 $m.s^{-1}$. However, according to the wind observations, the zonal wind dropped over a larger altitude range than the one where the temperature increased. Therefore, this computed zonal wind fluctuation is lower than the one observed, which is, in reality, around 150 $m.s^{-1}$ (Figure 2). Consequently, these computed zonal wind amplitudes possess uncertainties due to the employed method. These results illustrate the Doppler LiDAR's capacity to capture strong wind fluctuations over narrow layers. For instance, on 6 December 2021, a zonal wind deceleration of 105.5 ± 57.5 $m.s^{-1}$ associated with a temperature elevation of 29.5 ± 19.2 K are computed over a layer of 1.65 km. Finally, the MIL events on 12 December 2021 and 31 January 2020, respectively, possess temperature elevations of 6.5 ± 2.9 K and 46.8 ± 14.3 K associated with zonal wind decelerations of 34.3 ± 10.1 $m.s^{-1}$ and 59.4 ± 68.7 $m.s^{-1}$. These computed values confirm, unlike those above Biscarrosse, that large temperature amplitudes within MILs tend to be directly related to substantial wind deceleration. Thus, over these six MIL events, we found a mean temperature gradient of 7.5 $K.km^{-1}$ associated with a mean zonal wind deceleration gradient of 21 $m.s^{-1}.km^{-1}$.

On 3 December 2021, a second MIL was present at 75 km in the temperature profile, but the altitude range of the wind observations at this altitude does not allow to derive wind deceleration of this MIL. Despite this uncertainty, the Doppler LiDAR technique is an excellent instrument for documenting MIL's effects on winds. Finally, unlike the two MILs above Biscarrosse, ERA5 temperature and wind reanalyzes did not reproduce MILs' presence for these four dates above the OHP.

## 5. Discussion and Perspectives on Mechanisms Responsible for Lower MILs

From the above results concerning co-located temperature and wind observations in the mesosphere during MIL events (Figures 1 and 2), we can determine that MIL's formation involved systematic wind drops within the

altitude range where the temperature increases. Unfortunately, these results are insufficient to precisely determine how the zonal wind deceleration magnitude varies with a specific temperature increase. Indeed, the computed amplitudes possess several uncertainties, such as the possibility of observations carried out outside the MIL center and the presence of other geophysical processes. Moreover, the method employed here to characterize MILs is better suited for capturing temperature amplitudes than for capturing wind shears within MILs. Consequently, further simultaneous temperature-wind observations are necessary to quantify the wind-temperature interconnection accurately.

Among the reported existing mechanisms, the observed connection between temperature and wind supports the theory of MIL's formation mechanism, first introduced by Hauchecorne et al. (1987), which is based on breaking gravity waves inside a thin layer. Since the zonal wind is westerly at all altitudes from the troposphere to the mesosphere in winter, only gravity waves with a westward phase can propagate up to the mesosphere and break at a critical layer where the phase speed becomes close to the background wind (Lindzen, 1981). When a gravity wave breaks and dissipates, the associated momentum transfer decreases the zonal wind above the mesospheric jet, generating turbulence. This turbulence then produces downward vertical heat flux from the upper layer, which generates adiabatic warming responsible for temperature inversion. Thus, this generated turbulence layer favors a continuous breaking of gravity waves which can sustain a temperature inversion layer of tens of kelvins for several days. These perturbations that occur during a MIL event are illustrated in Figure 7 in Hauchecorne et al. (1987), with a schematic representation of the vertical profiles of the mean temperature and the mean zonal wind matching the observations reported in this article. Finally, the results found in Hauchecorne and Maillard (1990), who have simulated a temperature inversion with a 2D model that implies a wind drop by the breaking of gravity waves inside a thin layer, strengthen the notion that this mechanism is essential in MIL's formation.

The research done by Sassi et al. (2002) further supports this idea. The authors simulated a lower MIL events between 70 and 80 km at mid-latitudes with the breaking of planetary waves, which generates warming in the upper stratosphere and cooling in the lower mesosphere favorable toward MIL's appearance. Their analysis shows that such lower MIL events occur in a weak westward wind region produced by the deposition of momentum from westward gravity waves known to occur above 70 km (Mzé et al., 2014). Additionally, when they remove the gravity wave activity in their model, the positive temperature lapse rate created in the mesosphere disappears, confirming the crucial role of gravity waves in the lower MIL's formation and persistence.

Figure 1 shows that the ERA5 reanalyzes are sometimes able to simulate the wind deceleration phenomenon with similar magnitude to the observations reported here, whereas the temperature inversion is nearly overlooked. Nevertheless, for most cases, particularly over the OHP, Figure 2 shows that ERA5 reanalyzes did not capture temperature and wind fluctuations in the mesosphere during MIL events. As already discussed in Mariaccia et al. (2022), the coarse vertical resolution of the model at these altitudes prevent the simulation of such fluctuations. The authors also mention that, the bad representation of the mesosphere is enhanced by the lack of assimilated observation by the model at these altitudes. Furthermore, the sponge layer implemented in the model probably damps the gravity wave energy propagation up to the mesosphere which is necessary for MIL's apparition and sustainability. The realistic MIL characteristics statistics simulated by the Whole Atmosphere Community Climate Model (WACCM), which benefit from a better vertical resolution in the mesosphere than ERA5 (France et al., 2015), suggests that the resolution improvement is the first crucial step in the MIL's simulation achievement. Thus, the new results given above suggest that MIL's formation mechanisms should be considered as a first lead to pursue the elaboration of an accurate theory on the lower MIL's apparition. Future investigations are necessary to test how the energy transfer from gravity wave dissipation in the mesosphere can create background wind drops and temperature increases as those reported here. The elaboration of a new 3-D mechanistic model, in the same manner, that the one developed by Hauchecorne and Maillard (1990) should be pursued, but with a better vertical resolution to simulate temperature inversions by reducing locally wind.

However, the instrumental error associated with the Rayleigh LiDAR grows less quickly than for the Ozone LiDAR. This result is expected, as the Ozone LiDAR was not designed for measuring temperature. Similarly, the Doppler LiDAR observations still suffer from large instrumental errors in the higher mesosphere impacting the study of MIL's effects on zonal wind. Therefore, in order to improve our description of the MIL phenomenon, more wind observations performed by LIOwind Doppler LiDAR with meridional winds are required in addition to temperature measurements to benefit more extensive statistics of simultaneous wind temperature. Furthermore, the improvement of this technique to reduce instrumental errors in the upper mesosphere should

be pursued. Finally, the development of technical instruments capable of measuring the turbulence generated by gravity waves within MILs should be undertaken (Hauchecorne et al., 2016).

## Data Availability Statement

The OHP ground-based lidar data can be obtained via NDACC lidar database https://ndacc.larc.nasa.gov/. The indications to download the ERA-5 data over 137 levels are given on the ECWMF website https://confluence.ecmwf.int/display/CKB/How+to+download+ERA5.

**Acknowledgments**
We gratefully thank the personnel of Station Gerard Megie at OHP (Frederic Gomez, Francois Dolon, Francois Huppert and others) for conducting the lidar observations. The work related to Aeolus validation has been performed in the frame of Aeolus Scientific Calibration & Validation Team (ACVT) activities under support of CNES Aeolus project. The temperature measurements have been obtained as part of as part of the Network for the Detection of Atmospheric Composition Change (NDACC). The falling sphere data as well as the lidar data from Centre d'Essai des Landes (CEL) have been acquired in the frame of the DYANA campaign implying Direction Générale de l'Armement (DGA). This work was performed within the framework of the European ARISE project and was funded by the French Educational Ministry with EUR IPSL.

## References

Ardalan, M., Keckhut, P., Hauchecorne, A., Wing, R., Meftah, M., & Farhani, G. (2022). Updated climatology of mesospheric temperature inversions detected by Rayleigh lidar above observatoire de haute Provence, France, using a k-mean clustering technique. *Atmosphere*, *13*(5), 814. https://doi.org/10.3390/atmos13050814

Baumgarten, G. (2010). Doppler Rayleigh/Mie/Raman lidar for wind and temperature measurements in the middle atmosphere up to 80 km. *Atmospheric Measurement Techniques*, *3*(6), 1509–1518. https://doi.org/10.5194/amt-3-1509-2010

Chanin, M.-L., Garnier, A., Hauchecorne, A., & Porteneuve, J. (1989). A Doppler lidar for measuring winds in the middle atmosphere. *Geophysical Research Letters*, *16*(11), 1273–1276. https://doi.org/10.1029/gl016i011p01273

Cutler, L. J., Collins, R. L., Mizutani, K., & Itabe, T. (2001). Rayleigh lidar observations of mesospheric inversion layers at poker flat, Alaska (65 n, 147 w). *Geophysical Research Letters*, *28*(8), 1467–1470. https://doi.org/10.1029/2000gl012535

Dao, P. D., Farley, R., Tao, X., & Gardner, C. S. (1995). Lidar observations of the temperature profile between 25 and 103 km: Evidence of strong tidal perturbation. *Geophysical Research Letters*, *22*(20), 2825–2828. https://doi.org/10.1029/95gl02950

Duck, T. J., Sipler, D. P., Salah, J. E., & Meriwether, J. W. (2001). Rayleigh lidar observations of a mesospheric inversion layer during night and day. *Geophysical Research Letters*, *28*(18), 3597–3600. https://doi.org/10.1029/2001gl013409

Engler, N. A. (1965). *Development of methods to determine winds, density, pressure, and temperature from the robin falling balloon*. (Tech. Rep.). Dayton University Ohio Research Institute.

Fechine, J., Wrasse, C., Takahashi, H., Mlynczak, M., & Russell, J. (2008). Lower-mesospheric inversion layers over Brazilian equatorial region using timed/saber temperature profiles. *Advances in Space Research*, *41*(9), 1447–1453. https://doi.org/10.1016/j.asr.2007.04.070

France, J., Harvey, V., Randall, C., Collins, R., Smith, A., Peck, E., & Fang, X. (2015). A climatology of planetary wave-driven mesospheric inversion layers in the extratropical winter. *Journal of Geophysical Research: Atmospheres*, *120*(2), 399–413. https://doi.org/10.1002/2014jd022244

Gan, Q., Zhang, S. D., & Yi, F. (2012). Timed/saber observations of lower mesospheric inversion layers at low and middle latitudes. *Journal of Geophysical Research*, *117*(D7). https://doi.org/10.1029/2012jd017455

Garnier, A., Chanin, M. L., Hauchecorne, A., & Porteneuve, J. C. (1992). Laser device for measuring wind speeds at medium altitudes by using a Doppler effect. (US Patent 5,088,815).

Godin-Beekmann, S., Porteneuve, J., & Garnier, A. (2003). Systematic dial lidar monitoring of the stratospheric ozone vertical distribution at observatoire de haute-Provence (43.92 n, 5.71 e). *Journal of Environmental Monitoring*, *5*(1), 57–67. https://doi.org/10.1039/b205880d

Hauchecorne, A., Chanin, M.-L., & Keckhut, P. (1991). Climatology and trends of the middle atmospheric temperature (33–87 km) as seen by Rayleigh lidar over the south of France. *Journal of Geophysical Research*, *96*(D8), 15297–15309. https://doi.org/10.1029/91jd01213

Hauchecorne, A., Chanin, M. L., & Wilson, R. (1987). Mesospheric temperature inversion and gravity wave breaking. *Geophysical Research Letters*, *14*(9), 933–936. https://doi.org/10.1029/GL014i009p00933

Hauchecorne, A., Cot, C., Dalaudier, F., Porteneuve, J., Gaudo, T., Wilson, R., et al. (2016). Tentative detection of clear-air turbulence using a ground-based Rayleigh lidar. *Applied Optics*, *55*(13), 3420–3428. https://doi.org/10.1364/AO.55.003420

Hauchecorne, A., & Maillard, A. (1990). A 2-d dynamical model of mesospheric temperature inversions in winter. *Geophysical Research Letters*, *17*(12), 2197–2200. https://doi.org/10.1029/GL017i012p02197

Hersbach, H., Bell, B., Berrisford, P., Hirahara, S., Horányi, A., Muñoz-Sabater, J., et al. (2020). The ERA5 global reanalysis. *Quarterly Journal of the Royal Meteorological Society*, *146*(730), 1999–2049. https://doi.org/10.1002/qj.3803

Huang, T.-Y., Hickey, M. P., Tuan, T.-F., Dewan, E. M., & Picard, R. H. (2002). Further investigations of a mesospheric inversion layer observed in the aloha-93 campaign. *Journal of Geophysical Research*, *107*(D19), ACL17-1–ACL17-8. https://doi.org/10.1029/2001JD001186

Huang, T. Y., Hur, H., Tuan, T. F., Li, X., Dewan, E. M., & Picard, R. H. (1998). Sudden narrow temperature-inversion-layer formation in aloha-93 as a critical-layer-interaction phenomenon. *Journal of Geophysical Research*, *103*(D6), 6323–6332. https://doi.org/10.1029/97JD03076

Jones, L. M., & Peterson, J. W. (1968). Falling sphere measurements, 30 to 120 km. In R. S. Quiroz (Ed.), *Meteorological investigations of the upper atmosphere: Proceedings of the American meteorological society symposium on meteorological investigations above 70 kilometers, Miami beach, Florida, 31 May–2 June 1967* (pp. 176–189). American Meteorological Society. https://doi.org/10.1007/978-1-935704-37-9_21

Khaykin, S. M., Hauchecorne, A., Wing, R., Keckhut, P., Godin-Beekmann, S., Porteneuve, J., et al. (2020). Doppler lidar at observatoire de haute-Provence for wind profiling up to 75 km altitude: Performance evaluation and observations. *Atmospheric Measurement Techniques*, *13*(3), 1501–1516. https://doi.org/10.5194/amt-13-1501-2020

Leblanc, T., & Hauchecorne, A. (1997). Recent observations of mesospheric temperature inversions. *Journal of Geophysical Research*, *102*(D16), 19471–19482. https://doi.org/10.1029/97jd01445

Leblanc, T., Hauchecorne, A., Chanin, M.-L., Rodgers, C., Taylor, F., & Livesey, N. (1995). Mesospheric temperature inversions as seen by ISAMS in December 1991. *Geophysical Research Letters*, *22*(12), 1485–1488. https://doi.org/10.1029/94gl03274

Leblanc, T., McDermid, I. S., Keckhut, P., Hauchecorne, A., She, C. Y., & Krueger, D. A. (1998). Temperature climatology of the middle atmosphere from long-term lidar measurements at middle and low latitudes. *Journal of Geophysical Research*, *103*(D14), 17191–17204. https://doi.org/10.1029/98JD01347

Le Du, T., Keckhut, P., Hauchecorne, A., & Simoneau, P. (2022). Observation of gravity wave vertical propagation through a mesospheric inversion layer. *Atmosphere*, *13*(7), 1003. https://doi.org/10.3390/atmos13071003

Lindzen, R. S. (1981). Turbulence and stress owing to gravity wave and tidal breakdown. *Journal of Geophysical Research*, *86*(C10), 9707–9714. https://doi.org/10.1029/jc086ic10p09707

Liu, H.-L., & Hagan, M. E. (1998). Local heating/cooling of the mesosphere due to gravity wave and tidal coupling. *Geophysical Research Letters*, *25*(15), 2941–2944. https://doi.org/10.1029/98gl02153

Lübken, F.-J., Hillert, W., Lehmacher, G., Zahn, U., Bittner, M., Offermann, D., et al. (1994). Intercomparison of density and temperature profiles obtained by lidar, ionization gauges, falling spheres, datasondes and radiosondes during the DYANA campaign. *Journal of Atmospheric and Terrestrial Physics*, *56*(13), 1969–1984. (Dynamic Adapted Network for the the Atmosphere). https://doi.org/10.1016/0021-9169(94)90023-X

Mariaccia, A., Keckhut, P., Hauchecorne, A., Claud, C., Le Pichon, A., Meftah, M., & Khaykin, S. (2022). Assessment of ERA-5 temperature variability in the middle atmosphere using Rayleigh lidar measurements between 2005 and 2020. *Atmosphere*, *13*(2), 242. https://doi.org/10.3390/atmos13020242

Meriwether, J. W., & Gardner, C. S. (2000). A review of the mesosphere inversion layer phenomenon. *Journal of Geophysical Research*, *105*(D10), 12405–12416. https://doi.org/10.1029/2000jd900163

Meriwether, J. W., & Gerrard, A. J. (2004). Mesosphere inversion layers and stratosphere temperature enhancements. *Reviews of Geophysics*, *42*(3). https://doi.org/10.1029/2003RG000133

Meriwether, J. W., & Mlynczak, M. G. (1995). Is chemical heating a major cause of the mesosphere inversion layer? *Journal of Geophysical Research*, *100*(D1), 1379–1387. https://doi.org/10.1029/94jd01736

Mzé, N., Hauchecorne, A., Keckhut, P., & Thétis, M. (2014). Vertical distribution of gravity wave potential energy from long-term Rayleigh lidar data at a northern middle-latitude site. *Journal of Geophysical Research: Atmospheres*, *119*(21), 12069–12083. https://doi.org/10.1002/2014JD022035

Offermann, D. (1994). The DYANA campaign: A survey. *Journal of Atmospheric and Terrestrial Physics*, *56*(13), 1639–1657. (Dynamic Adapted Network for the the Atmosphere). https://doi.org/10.1016/0021-9169(94)90002-7

Ramesh, K., Sridharan, S., & Vijaya Bhaskara Rao, S. (2013). Dominance of chemical heating over dynamics in causing a few large mesospheric inversion layer events during January–February 2011. *Journal of Geophysical Research: Space Physics*, *118*(10), 6751–6765. https://doi.org/10.1002/jgra.50601

Ratynski, M., Khaykin, S., Hauchecorne, A., Wing, R., Cammas, J.-P., Hello, Y., & Keckhut, P. (2022). Validation of Aeolus wind profiles using ground-based lidar and radiosonde observations at la Réunion Island and the observatoire de haute Provence. *EGUsphere*, 1–33. https://doi.org/10.5194/egusphere-2022-822

Salby, M., Sassi, F., Callaghan, P., Wu, D., Keckhut, P., & Hauchecorne, A. (2002). Mesospheric inversions and their relationship to planetary wave structure. *Journal of Geophysical Research*, *107*(D4), ACL4-1–ACL4-13. https://doi.org/10.1029/2001JD000756

Sassi, F., Garcia, R. R., Boville, B. A., & Liu, H. (2002). On temperature inversions and the mesospheric surf zone. *Journal of Geophysical Research*, *107*(D19), ACL8-1–ACL8-11. https://doi.org/10.1029/2001JD001525

Schmidlin, F. (1976). Temperature inversions near 75 km. *Geophysical Research Letters*, *3*(3), 173–176. https://doi.org/10.1029/gl003i003p00173

Souprayen, C., Garnier, A., Hertzog, A., Hauchecorne, A., & Porteneuve, J. (1999). Rayleigh–Mie Doppler wind lidar for atmospheric measurements. I. instrumental setup, validation, and first climatological results. *Applied Optics*, *38*(12), 2410–2421. https://doi.org/10.1364/AO.38.002410

Straume, A. G., Rennie, M., Isaksen, L., de Kloe, J., Marseille, G.-J., Stoffelen, A., et al. (2020). Esa´s space-based Doppler wind lidar mission Aeolus—First wind and aerosol product assessment results. *EPJ Web of Conferences*, *237*, 01007. https://doi.org/10.1051/epjconf/202023701007

Stroud, W. G., Nordberg, W., Bandeen, W. R., Bartman, F. L., & Titus, P. (1960). Rocket-grenade measurements of temperatures and winds in the mesosphere over Churchill, Canada. *Journal of Geophysical Research*, *65*(8), 2307–2323. https://doi.org/10.1029/JZ065i008p02307

Theon, J. S., Nordberg, W., Katchen, L. B., & Horvath, J. J. (1967). Some observations on the thermal behavior of the mesosphere. *Journal of the Atmospheric Sciences*, *24*(4), 428–438. https://doi.org/10.1175/1520-0469(1967)024⟨0428:SOOTTB⟩2.0.CO;2

Wing, R., Hauchecorne, A., Keckhut, P., Godin-Beekmann, S., Khaykin, S., McCullough, E. M., et al. (2018). Lidar temperature series in the middle atmosphere as a reference data set–part 1: Improved retrievals and a 20-year cross-validation of two co-located French lidars. *Atmospheric Measurement Techniques*, *11*(10), 5531–5547. https://doi.org/10.5194/amt-11-5531-2018

Wing, R., Martic, M., Hauchecorne, A., Porteneuve, J., Keckhut, P., Courcoux, Y., et al. (2020). Atmospheric density and temperature vertical profile retrieval for flight-tests with a Rayleigh lidar on-board the French advanced test range ship monge. *Atmosphere*, *11*(1), 75. https://doi.org/10.3390/atmos11010075